Fatigue Failure in Polysilicon Not Due to Simple Stress Corrosion Cracking

H. Kahn, R. Ballarini,* J. J. Bellante, A. H. Heuer*

In the absence of a corrosive environment, brittle materials such as silicon should be immune to cyclic fatigue. However, fatigue effects are well known in micrometer-sized polycrystalline silicon (polysilicon) samples tested in air. To investigate the origins of this phenomenon in polysilicon, we developed a fixed-grip fracture mechanics microspecimen but could find no evidence of static stress corrosion cracking. The environmental sensitivity of the fatigue resistance was also investigated under cyclic loading. For low-cycle fatigue, the behavior is independent of the ambient conditions, whether air or vacuum, but is strongly influenced by the ratio of compressive to tensile stresses experienced during each cycle. The fatigue damage most likely originates from contact stresses at processing-related surface asperities; subcritical crack growth then ensues during further cyclic loading. The lower far-field stresses involved in high-cycle fatigue induce reduced levels of fatigue damage. Under these conditions, a corrosive ambient such as laboratory air exacerbates the fatigue process. Without cyclic loading, polysilicon does not undergo stress corrosion cracking.

Silicon is a "fully" brittle material at room temperature. In the absence of hydrostatic confining pressures to suppress fracture, silicon displays no stress-induced dislocation activity under ambient conditions, even under high stresses, and undergoes no stress-induced phase transformations, except at extremely high pressures (*1*). In addition, stress corrosion cracking (*2*) has not been conclusively detected in silicon (*3*, *4*). We thus do not expect silicon to display any time-dependent cracking (neither crack initiation nor crack extension) when subjected to monotonic or cyclic loading conditions. Experimental results, however, have shown otherwise. Precracked micrometer-sized specimens of both single-crystal (*4*) and polycrystalline silicon (polysilicon) (*5*) exhibit crack extension when subjected to cyclic fatigue loading. Crack initiation and growth have also been observed in micrometer-sized silicon specimens without precracks under fatigue loading (*6*–*11*). Both single-crystal silicon (*6*, *7*) and polysilicon (*8*–*11*) have been studied. Most of the investigations (*6*–*10*) used equal tension/compression cycling, for a load ratio $R = -1$. (The load ratio R is the ratio of the minimum stress to the maximum stress in the cycle; tension is taken as positive and compression as negative.) Fatigue has also been observed in zero/tension stress cycling tests ($R = 0$) (*11*). Muhlstein *et al*. (*9*, *10*) have attributed the limited lifetime to "reaction-layer fatigue." This fatigue mechanism involves the surface oxide (*12*) on the silicon undergoing damage through stress corrosion cracking; the oxide is postulated to thicken because of continued chemical reaction with the ambient, and the cracks lengthen until the stress intensity factor reaches the critical fracture toughness K_{IC} (Eq. 1), whereupon catastrophic crack propagation ensues. Bagdahn *et al*. (*11*), however, showed that the lifetime of polysilicon specimens subjected to tensile fatigue loading was dependent only on the number of cycles and not on the cycling frequency.

In fact, stress corrosion is not a prerequisite for fatigue behavior in brittle materials. Suresh (*13*) showed that brittle ceramics display crack initiation and propagation at notches under compression/compression fatigue loading. He attributed the fatigue to confined damage at the notch tip during compression loading, which generates tensile stresses and microcracking upon unloading. Further, Wiederhorn *et al*. (*14*) reported temperature-dependent subcritical crack growth in a variety of inorganic glasses subjected to constant tensile loads in vacuum (10^{-2} Pa).

For our investigation, the test structure shown in Fig. 1 was used to investigate the static (constant load) stress corrosion of polysilicon in micrometer-sized specimens. The fracture mechanics microspecimen, a doubly clamped beam with a residual tensile stress and containing a sharp precrack produced by a Vickers microindent, was fabricated with standard micromachining techniques (*15*). Upon release of the structure, the residual tensile stress in the film produced a nearly uniform tensile stress in the doubly clamped beam and, in turn, a well-defined stress intensity at the crack tip. The residual stress in the film was measured with microstrain gauges, which were micromachined on the same substrate and placed near the test devices. We

Case Western Reserve University, 10900 Euclid Avenue, Cleveland, OH 44106–7204, USA.

*To whom correspondence should be addressed: E-mail: rxb7@po.cwru.edu (R.B.); ahh@po.cwru.edu (A.H.H.)

References and Notes

1. J. B. Neaton, N. W. Ashcroft, *Nature* **400**, 141 (2000).
2. M. Hanfland, K. Syassen, N. E. Christensen, D. L. Novikov, *Nature* **408**, 174 (2000).
3. A. W. Overhauser, *Phys. Rev. Lett.* **53**, 64 (1984).
4. K. M. Lang *et al.*, *J. Low Temp. Phys.* **114**, 445 (1999).
5. N. W. Ashcroft, in *Proceedings of the International School of Physics "Enrico Fermi,"* R. J. Hemley, G. Chiarotti, M. Bernasconi, L. Ulivi, Eds., vol. **CXLVII**, in press.
6. N. E. Christensen, D. L. Novikov, *Phys. Rev. Lett.* **86**, 1861 (2001).
7. T. H. Lin, K. J. Dunn, *Phys. Rev. B* **33**, 807 (1986).
8. K. Shimizu, private communication.
9. V. V. Struzhkin, R. J. Hemley, H. K. Mao, *Bull. Am. Phys. Soc.* **44**, 1489 (1999).
10. Yu. A. Timofeev, V. V. Struzhkin, R. J. Hemley, H. K. Mao, E. Gregoryanz, *Rev. Sci. Instrum.* **73**, 371 (2002).
11. M. I. Eremets, V. V. Struzhkin, H. K. Mao, R. J. Hemley, *Science* **293**, 272 (2001).
12. Materials and methods are available as supporting material on *Science* Online.
13. E. Gregoryanz *et al.*, *Phys. Rev. B* **65**, 064504 (2002).
14. C. F. Richardson, N. W. Ashcroft, *Phys. Rev. B,* **55**, 15130 (1997).
15. D. G. Hinks, H. Claus, J. D. Jorgensen, *Nature* **411**, 457 (2001).
16. R. J. Nelmes, M. I. McMahon, J. S. Loveday, S. Rekhi, *Phys. Rev. Lett.* **88**, 155503 (2002).
17. J. S. Tse, private communication.
18. C. F. Richardson, N. W. Ashcroft, *Phys. Rev. Lett,* **78**, 118 (1997).
19. K. Moulopoulos, N.W. Ashcroft, *Phys. Rev. B* **59**, 12309 (1999).
20. Supported by the DOE grant #DEFG02-02ER45955, the NSF (DMR-0205899), and the W. M. Keck Foundation. W.G. acknowledges support from REU Site for Undergraduate Research Training in Geoscience (NSF EAR-0097569), W. G. Minarik, and S. B. Shirey. We thank J. Schilling and J. Tse for useful comments and discussions.

Supporting Online Material
www.sciencemag.org/cgi/content/full/1078535/DC1
Materials and Methods

18 September 2002; accepted 7 October 2002
Published online 17 October 2002;
10.1126/science.1078535
Include this information when citing this paper.

have characterized the residual (growth) stresses generated in low-pressure chemical vapor deposition (LPCVD) polysilicon films in considerable detail (*16*), and we produced films with residual tensile stresses suitable for this experiment (*17*). Because of the stochastic nature of microindentation, the crack length (*a* in Fig. 1A) varied from specimen to specimen, even though essentially identical indentation conditions were used. As a result, a range of stress intensities was produced. Upon release of the microdevices, growth occurred in cracks whose stress intensity factor K was greater than K_{IC}, whereas growth did not occur in cracks whose K was lower than K_{IC}. For our experiment, three polysilicon films were used, with residual stresses of 69, 56, and 44 MPa. K versus a curves for each film were determined from finite element analyses and are shown in Fig. 1D, along with the experimental data (*18*). Except for one outlier at a crack length of 38 μm in the film with a residual stress of 44 MPa, the three sets of data show upper and lower bounds for K_{IC}. The combined results give $K_{IC} = 0.81 \pm 0.05$ MPa · $m^{1/2}$. This value is consistent with previously reported data for bulk polysilicon (*19*) and is slightly less than our previously reported data (*20*).

The beams represented by squares in Fig. 1D contain cracks whose stress intensities (0.49 to 0.82 MPa · $m^{1/2}$) are slightly less than K_{IC}. The loads due to the residual stresses on these cracks are constant, and these beams are therefore ideal specimens for studying static stress corrosion cracking. These polysilicon beams were placed in a 90% relative humidity chamber for 30 days. None of the cracks in the beams grew. The spatial resolution in imaging crack length with scanning electron microscopy is 0.1 μm. Therefore, subcritical crack growth could not have involved crack velocities greater than 4×10^{-14} m/s.

We also investigated crack initiation and growth during both monotonic and cyclic loading, with the polysilicon microdevices shown in Fig. 2. Devices were fabricated from two different polysilicon films, with thicknesses of 3.5 and 6.0 μm. After release, a 10-nm-thick film of palladium was sputtered onto the devices to create sufficient conductivity for electrostatic loading. For this experiment, the polysilicon films were annealed before patterning to reduce residual stresses to near zero.

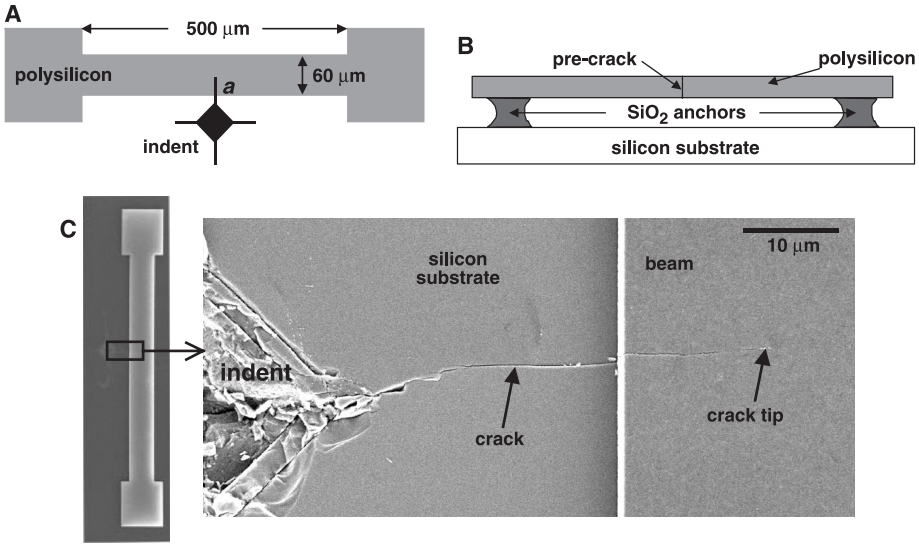

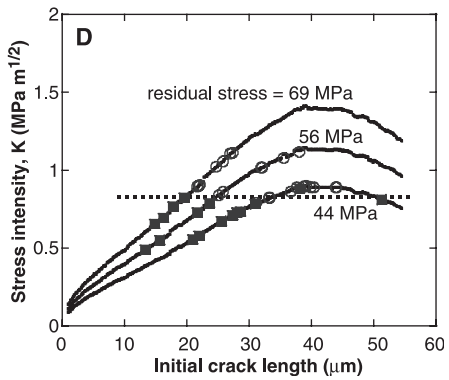

Fig. 1. Images of the doubly clamped tensile beam used to measure fracture toughness and stress corrosion. (**A**) Schematic top view showing the dimensions. (**B**) Schematic side view. (**C**) Scanning electron micrograph (SEM) of a 60-μm-wide beam with an indent placed near its center, with a higher magnification SEM of the area near the indent showing the precrack traveling from the substrate into the beam. The indent was made on the SiO_2 release layer, which was subsequently removed by the HF release acid. (**D**) Plot of stress intensity K versus crack length a for polysilicon doubly clamped tensile beams. The solid lines show the relation between K and a for three values of residual stress; the data points are shown as symbols (squares, cracks that did not grow upon release; circles, cracks that did grow). The dotted line indicates the fracture toughness K_{IC}, determined from these data.

The electrostatic comb-drive actuator shown in Fig. 2 has been described previously (*8*). It allows constant, monotonically increasing, or cyclic loading, depending on whether dc or ac voltages are applied. (The resonance frequencies of these devices are ~10 kHz.) Further, cyclic loading can be superimposed on a mean stress by adding an ac voltage to a dc bias.

With the single edge-notched microspecimen shown in Fig. 2B, a dc voltage applied to the actuator generated a tensile stress at the notch tip. As the dc voltage was increased, the tensile stress increased until it exceeded the strength of the polysilicon, at which point a crack was initiated and catastrophically propagated through the uncracked ligament. The stresses at the notch tip were determined with finite element analysis of the microdevice, in conjunction with direct measurements of the actuator displacement. The average bend strength in air (nominally 23°C at 25 to 35% relative humidity under monotonic loading) taken from nine specimens was 4.0 GPa, with a standard deviation of 0.6 GPa.

To determine whether "natural" flaws (as opposed to the indent-induced microcracks) (Fig. 1C) could undergo environmentally assisted subcritical crack growth, we subjected 10 specimens to a constant tensile stress in air of 3.6 GPa (*21*). (The relevance of this stress level will become clear in the context of Fig. 3D.) The devices were exposed to laboratory air for 2 hours and then placed in a 90% relative humidity chamber for 200 hours. No failures were observed. Combined with the very low crack velocities implied by the doubly clamped beam experiments (Fig. 1), this negative result demonstrates that silicon is not susceptible to static stress corrosion cracking.

We next investigated the relative importance of compressive and tensile stresses during cyclic loading and subjected polysilicon specimens to fatigue tests with varying R values. Because the electrostatic actuator can apply monotonic loading in only one direction (downward, as oriented in Fig. 2), the two different single edge-notched fracture mechanics microspecimens shown in Fig. 2, B and C, were designed. The notch root radius was 1.1 μm for both specimens. For the specimen in Fig. 2B, as described above, the monotonic component of the load created a tensile stress at the notch tip, and for the specimen shown in Fig. 2C, it created a compressive stress. Depending on the choice of specimen and the magnitude of monotonic load, fatigue tests can be performed with varying R values.

For both specimen types, we applied a dc bias voltage and a small ac voltage and determined the resonance frequency (*22*). Holding the frequency of the ac signal at resonance, we slowly increased the amplitude of the applied ac voltage until fracture occurred. Typically, the entire test lasted less than 1 min. This test

revealed the conditions that result in low-cycle fatigue (*23*). Because brittle materials such as silicon have a much lower strength in tension than in compression, bend specimens invariably fail from cracks nucleated at or near the tensile side of the beam. We therefore presume that the maximum tensile stress experienced at the notch tip during the fatigue cycle is the low-cycle fatigue strength and is equal to the critical tensile stress required for catastrophic crack propagation σ_{crit}. Tests were performed at atmospheric pressure (10^5 Pa) and in vacuum (10 Pa). The results are shown in Fig. 3A, where fatigue strength is plotted versus R.

It is evident that the polysilicon specimens are susceptible to fatigue; in the absence of fatigue damage, the fatigue strength would be constant, equal to the monotonic bend strength, and independent of R. On the contrary, as R increases from large negative values, σ_{crit} increases. The failure stress is related to the fracture toughness of the material by the standard relation

$$K_{IC} = k\sigma_{crit}(\pi c)^{1/2} \quad (1)$$

where c is the size of the crack-initiating flaw and k is a constant of order unity (*24*). Because K_{IC} has been shown to be a microstructure-independent constant for polysilicon (*25*), the decrease in σ_{crit} with decreasing R must be due to increasing flaw sizes (*26*). All specimens from a given polysilicon film were fabricated simultaneously, so the flaw populations should be identical. It therefore follows that the specimens subjected to fatigue loading with the larger negative R values experienced enhanced subcritical crack growth.

To confirm that more extensive subcritical crack growth occurred at the lower R values, we examined fracture surfaces of several specimens (Fig. 3, B and C). The specimen in Fig. 3B was fatigued with $R = -0.4$ and fractured at $\sigma_{crit} = 3.4$ GPa, and the specimen in Fig. 3C was fatigued with $R = -2.1$ and fractured at $\sigma_{crit} = 1.7$ GPa. The fracture surfaces exhibit the classic morphology of brittle fracture: a relatively smooth, semicircular "mirror" region emanating from the fracture origin and a rougher surface characteristic of branching cracks beyond the mirror zone. The mirror radius is directly proportional to the crack-initiating flaw size. The mirror radius in Fig. 3C is roughly four times the mirror radius in Fig. 3B, consistent with the factor of 2 difference in measured strength (Eq. 1). This confirms that a greater amount of subcritical crack growth occurred in the specimen loaded with the larger negative R.

The data taken at the two different ambient pressures are indistinguishable (Fig. 3A), indicating that environmental effects, including possible oxidation-induced stress corrosion, do not affect the low-cycle fatigue behavior. Rather, the fatigue behavior must reflect irreversible processes occurring at the notch tip during cyclic loading. The severity of the fatigue damage is strongly affected by the compressive stresses experienced during fatigue loading. This suggests that the mechanism responsible for fatigue is similar to that proposed by Suresh (*13*) for compression/compression fatigue of brittle ceramics. A likely origin of the microcracks that

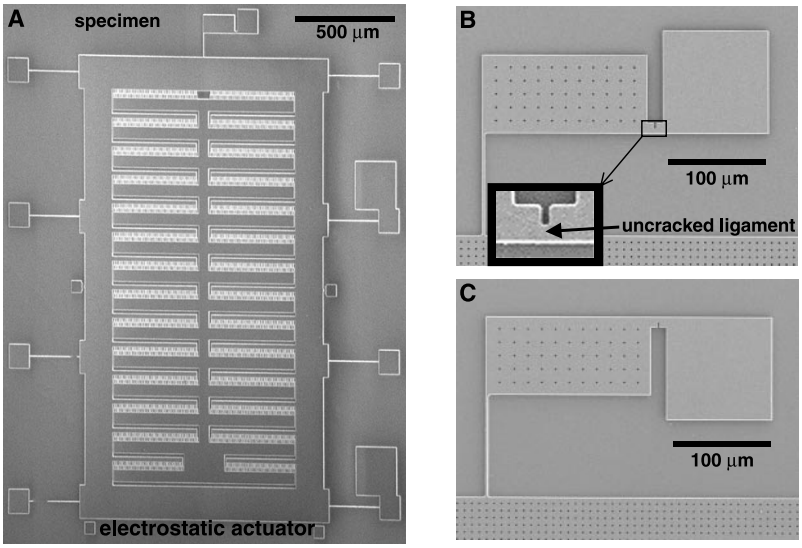

Fig. 2. SEMs of the polysilicon device used for monotonic and fatigue investigations. (**A**) The fracture mechanics specimen attached to the electrostatic comb-drive microactuator. (**B** and **C**) Higher magnification images of the two different single edge-notched fracture mechanics specimens used. The specimen in (B) allows monotonic tensile loads at the notch tip, producing R ratios greater than –1; the specimen in (C) allows monotonic compressive loads at the notch tip, producing R ratios less than –1. The inset in (B) shows a higher magnification view of the vicinity of the micromachined notch.

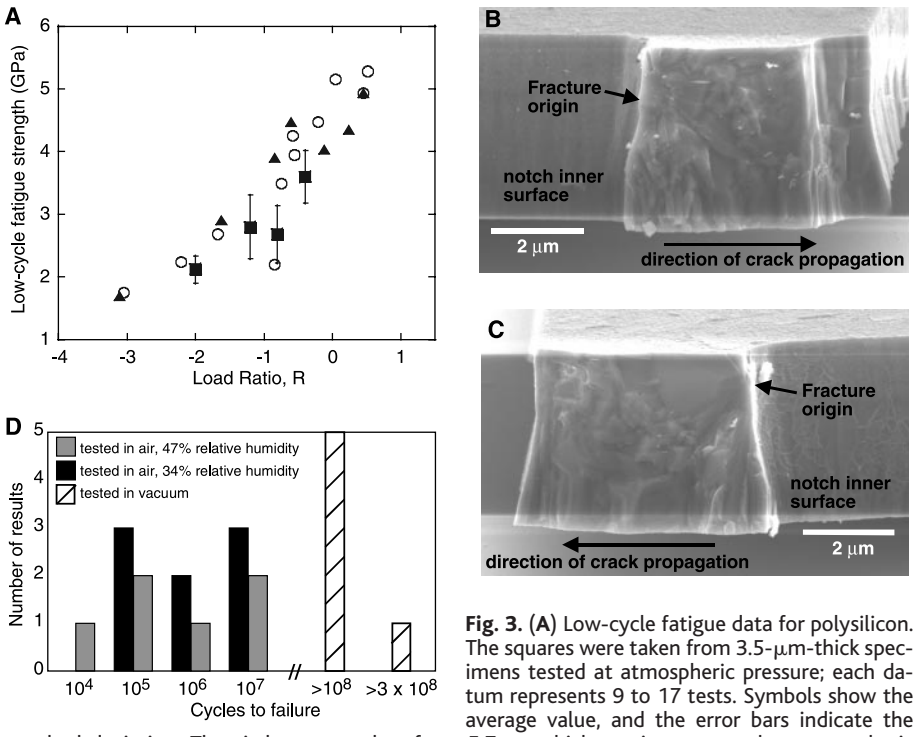

Fig. 3. (**A**) Low-cycle fatigue data for polysilicon. The squares were taken from 3.5-μm-thick specimens tested at atmospheric pressure; each datum represents 9 to 17 tests. Symbols show the average value, and the error bars indicate the standard deviation. The circles were taken from 5.7-μm-thick specimens tested at atmospheric pressure. The triangles were taken from 5.7-μm-thick specimens tested in vacuum (10 Pa). (**B** and **C**) SEMs showing the fracture surfaces of two specimens. The specimen in (B) is of the type shown in Fig. 2B; it was subjected to a tensile bias stress ($R = -0.4$) when resonated, and it fractured at a maximum stress of 3.4 GPa. The specimen in (C) is of the type shown in Fig. 2C; it was subjected to a compressive bias stress ($R = -2.1$) when resonated, and it fractured at a maximum stress of 1.7 GPa. (**D**) Histogram showing high-cycle fatigue results. Testing was done both in vacuum and in air, at two different relative humidities. Test conditions were $R = -0.5$, with a maximum stress of 3.6 GPa. No failures were observed in the six vacuum tests. Five of these tests were stopped after 10^8 cycles, and one was stopped after 3×10^8 cycles.

undergo subcritical crack growth in our specimens is the asperities on the notch surfaces, which can come into contact during the compressive cycles and which then act as "wedges" to create areas of local tension. The morphology of the micromachined inner notch surfaces is determined by the plasma etching of the polysilicon in the final stages of microelectromechanical systems (MEMS) processing (*15*) (Fig. 3, B and C). These surfaces display visible roughness, including surface asperities, although no microcracking could be observed by scanning electron microscopy. However, any microcracks would likely be closed after specimen fracture and therefore difficult to image. Accumulation of fatigue damage from this mechanism could be expected to depend on the number of cycles and not on the cycling frequency, as has been observed (*11*).

We were able to demonstrate the effects of environment on this fatigue mechanism during long-term, high-cycle fatigue tests. We measured the high-cycle fatigue life of specimens of the type shown in Fig. 2B, using the methodology just described, except that the amplitude of the applied ac voltage was held constant at a level slightly below that required for low-cycle fatigue failure; we tested in both laboratory air (10^5 Pa) and in vacuum (10 Pa). The specimens were tested with $R = -0.5$ and a maximum tensile stress of 3.6 GPa. All of the specimens tested in air failed catastrophically at 3.0×10^7 cycles or less (1.1 hours or less), whereas all of the specimens tested in vacuum survived at least 10^8 cycles (3.5 hours or more), when the vacuum tests were terminated (Fig. 3D). The ambient air clearly exacerbated the compression-induced (mechanical) fatigue mechanism. The presence of air may have caused an additional thickness of surface oxide to grow on existing asperities or on newly formed (subcritical) crack surfaces, which generated additional wedging and crack extension during the compressive portions of the loading cycle. When fatigue experiments are conducted involving compressive stresses that are less severe than those used in the lowcycle fatigue tests, the severity of cyclic fatigue damage depends sensitively on the ambient.

We demonstrated that without cyclic loading, stress corrosion cracking does not occur in polysilicon. Low-cycle fatigue damage in polysilicon is not affected by ambient conditions and most likely involves local microcracking at the notch tip owing to compressive stresses during the loading cycles. The extent of such damage is sensitive to the type and extent of surface roughness introduced during device fabrication. Under the low-cycle fatigue conditions, the fatigue damage occurs so quickly that it is not sensitive to ambient conditions. For high-cycle fatigue, a corrosive ambient, laboratory air, exacerbates the fatigue process.

References and Notes

1. J. C. Jamieson, *Science* **139**, 762 (1963).
2. Stress corrosion cracking (sometimes called "static fatigue" in the ceramics literature) is the propagation of a sharp crack in a brittle solid under an applied stress too low for catastrophic fracture and in the presence of a corrosive environment. In the case of silica glass, for which the existence of stress corrosion in the presence of humidity is well established, the ambient H_2O molecules react with crack-bridging Si-O-Si bonds and create two Si-O-H surface groups, with localized crack extension (*27*).
3. A. M. Fitzgerald, R. S. Iyer, R. H. Dauskardt, T. W. Kenny, *J. Mater. Res.* **17**, 683 (2002).
4. J. A. Connally, S. B. Brown, *Science* **256**, 1537 (1992).
5. W. W. Van Arsdell, S. B. Brown, *J. Microelectromech. Syst.* **8**, 319 (1999).
6. T. Tsuchiya *et al.*, *Tech. Dig. Sensor Symp.* **16**, 277 (1998).
7. C. L. Muhlstein, S. B. Brown, R. O. Ritchie, *J. Microelectromech. Syst.* **10**, 593 (2001).
8. H. Kahn, R. Ballarini, R. L. Mullen, A. H. Heuer, *Proc. R. Soc. London Ser. A* **455**, 3807 (1999).
9. C. L. Muhlstein, S. B. Brown, R. O. Ritchie, *Sens. Actuators A* **94**, 177 (2001).
10. C. L. Muhlstein, E. A. Stach, R. O. Ritchie, *Appl. Phys. Lett.* **80**, 1532 (2002).
11. J. Bagdahn, J. Schischka, M. Petzold, W. N. Sharpe Jr., *Proc. SPIE* **4558**, 159 (2001).
12. The growth of a thin oxide layer on silicon at room temperature, sometimes called a "native oxide," is well established (*28*). It typically becomes ~2 nm thick after exposure to air and gradually thickens to a maximum of ~4 nm.
13. S. Suresh, *Intl. J. Fract.* **42**, 41 (1990).
14. S. M. Wiederhorn, H. Johnson, A. M. Diness, A. H. Heuer, *J. Am. Ceram. Soc.* **57**, 336 (1974).
15. Micromachining is used in the sense common in the MEMS literature. Release during micromachining refers to the dissolution of the sacrificial SiO_2 layer beneath the fabricated structures, which allows portions of a device to be free from the substrate while remaining anchored at discrete points. The details of our MEMS fabrication can be found in (*8*).
16. J. Yang, H. Kahn, S. M. Phillips, A. H. Heuer, *J. Microelectromech. Syst.* **9**, 485 (2000).
17. Three polysilicon films were used in this investigation. Two were 3.0 μm thick and deposited with LPCVD at 580°C. This deposition temperature results in an as-deposited residual tensile stress of ~300 MPa. The first film was annealed at 910°C in argon, and the residual stress was reduced to 69 MPa. The second film was annealed for a longer time at 910°C in argon, and the residual stress was reduced to 56 MPa. The third polysilicon film was a 3.7-μm-thick multilayer and consisted of nine layers, each between 0.2 and 0.8 μm thick. This film was deposited at alternating temperatures of 570° and 615°C, as described in (*16*). The layers deposited at 570°C contained tensile residual stresses on the order of 300 MPa, and the layers deposited at 615°C contained compressive residual stresses, also on the order of 300 MPa. The overall residual stress of the as-deposited multilayer was 69 MPa, but after annealing at 1000°C in nitrogen, the overall residual stress decreased to 44 MPa. The stresses of the individual layers probably differ from the overall value. However, these local stresses do not affect the behavior of the crack tips in these multilayer polysilicon films, as was confirmed by fracture toughness investigations of polysilicon films of varying microstructures, as described in (*25*).
18. The finite element analysis assumes a perfectly straight precrack perpendicular to the beam axis, with a perfectly vertical crack front. As seen in Fig. 1C, the precrack paths are not perfectly straight; some deviate by as much as approximately ±5° from the beam normal. The faces of the original precracks were viewed postmortem. We found that the precrack fronts were often slightly curved. Also, some of the crack paths had tilted and lay at an angle through the beam thickness, again by approximately ±5°. These deviations from the assumed crack shape were estimated to affect the calculations of K by, at most, a few percent. The fact that the K versus a curves of Fig. 1D theoretically fall to zero as the crack reaches the free surface implies that crack arrest can occur after a finite amount of crack propagation, when K falls below K_{IC}. However, the region where K falls below K_{IC} is extremely small for the 56- and 69-MPa specimens; therefore, these did not exhibit crack arrest. Four of the 44-MPa specimens exhibited crack arrest after propagation distances of 38, 44, 46, and 56 μm, because for these the stress intensity factor only slightly exceeds K_{IC} and can easily drop below K_{IC} with modest crack extension.
19. C. P. Chen, M. H. Leipold, D. Helmreich, *J. Am. Ceram. Soc.* **65**, C-49 (1982).
20. We determined a microstructure-independent value of K_{IC} for amorphous silicon and polysilicon of several different microstructures of 1.0 ± 0.1 MPa · $m^{1/2}$ (*25*). All of these latter specimens had been tested in air, and the precrack surfaces must have contained a native oxide of ~2-nm thickness (*28*). By contrast, precrack surfaces in the present specimens had been created during the hydrofluoric acid (HF) release step (*8*) and were thus passivated by Si-H bonds (*29*). We suggest that the native oxide present in the specimens of (*25*) is responsible for the slightly higher K_{IC}.
21. The procedure for this experiment is described as follows. The actuators were mechanically displaced to produce a tensile stress at the notch tip of 3.6 GPa. Next, a dc voltage was applied between the actuator and the substrate, clamping the actuator to the substrate, and a drop of water was placed on the actuator. When the water evaporated, the capillary forces brought the actuator and substrate into intimate contact, generating van der Waals forces. These forces, sometimes referred to as "stiction" in the micromachining literature, are quite strong when compared to the size of the devices, and they secured the actuator permanently in place, even when the voltage was removed.
22. As the applied dc bias voltage causes the actuator to deflect, this increases the stiffness of the actuator support beams, causing small changes in the resonant frequency of the microdevice.
23. Although we use the term "low-cycle fatigue," the specimens experienced the fatigue stress conditions for up to several seconds, which corresponds to $\sim 5 \times 10^4$ cycles.
24. For a semicircular flaw, $k = 0.71$ (*30*).
25. R. Ballarini, H. Kahn, N. Tayebi, A. H. Heuer, in *Mechanical Properties of Structural Films*, *ASTM STP 1413*, C. L. Muhlstein, S. B. Brown, Eds. (American Society for Testing and Materials, West Conshohocken, PA, 2001), pp. 37–51.
26. Although the five specimens tested with $R > 0$ (tensile stresses only) appeared to exhibit strengths greater than the measured monotonic bend strength, these five data varied between 4.3 and 5.3 GPa. In comparison, the nine samples tested under monotonic loading had strengths between 3.0 and 4.8 GPa. We think that these differences are merely statistical and reflect the vagaries of processing brittle materials such as silicon; Eq. 1 indicates that the flaw size corresponding to a strength of 3.0 GPa is 35 nm, whereas the flaw size that corresponds to a strength of 5.3 GPa is 11 nm. When taken as a single population, the 14 measurements obey Weibull statistics, with a mean strength of 4.3 GPa and a Weibull modulus of 6.3.
27. T. A. Michalske, S. W. Freiman, *J. Am. Ceram. Soc.* **66**, 284 (1983).
28. S. K. Ghandi, *VLSI Fabrication Principles* (Wiley, New York, 1983), p. 373.
29. Y. A. Chabal, K. Raghavachari, *Surf. Sci.* **502–503**, 41 (2002).
30. I. S. Raju, J. C. Newman Jr., *Eng. Fract. Mech.* **11**, 817 (1979).

31. We thank Y. Wang for the finite element analysis of the doubly clamped beams. This work was supported by the Defense Advanced Research Projects Agency under contract N00014-00-1-0881.

10 July 2002; accepted 26 September 2002